

3D Eikonal Solvers, Part III: Amplitude Computation

Seongjai Kim*

Abstract

The amplitude computation requires an accurate approximation for the traveltime gradient and Laplacian. Since it is hard to compute the traveltimes with a second- or higher-order accuracy in realistic media, the difference approximations of the traveltime derivatives may not be suitable for accurate amplitudes unless special cares are taken. This article is concerned with a concurrent simulation of the traveltime and amplitude; strategies for accurate traveltimes and difference approximations of the traveltime derivatives are suggested to compute the amplitude with a positive-order accuracy. Second-order essentially non-oscillatory (ENO) schemes have been introduced for the traveltime Laplacian to compute the amplitude accurately. An ENO scheme for the traveltime second-derivative in the amplitude-marching direction is successfully designed incorporating the mid-step traveltime. To improve accuracy of the traveltime and amplitude particularly near the source, this article introduces a new family of second-order difference method, called *quadratic ENO* (QENO) scheme which approximates the traveltime derivatives *exactly* when the wavefront is circular or elliptical. The resulting algorithm integrating the new schemes and strategies turns out to show a second-order accuracy for the traveltime and a first-order accuracy for the amplitude in smooth regions.

1. Introduction

Imaging techniques based on high frequency asymptotic representation of the acoustic/elastic Green's function require efficient solution methods for the eikonal and transport equations for the computation of traveltimes and amplitudes. Finite difference (FD) algorithms solve the eikonal equation on regular grids with usable accuracy [2, 4, 7, 8, 9, 15, 16, 19, 23, 24]. Since the transport equation incorporates

*Department of Mathematics, University of Kentucky, Lexington, Kentucky 40506-0027 Email: skim@ms.uky.edu. The work is supported in part by NSF grant DMS-0107210.

the gradient and Laplacian of the traveltimes, both the traveltimes and the FD approximations of the traveltimes derivatives must be computed accurately enough to deliver a positive-order accuracy to the traveltimes Laplacian and therefore to the amplitude.

However, it is hard to keep a high-order accuracy for the traveltimes in realistic media. When shocks develop or the velocity is discontinuous, FD schemes (either first-order or higher-order) turn out to become first-order near the discontinuities and the FD traveltimes Laplacian can hardly show a positive-order accuracy. It has been observed that FD approximations of the traveltimes Laplacian often become oscillatory across discontinuities of either the velocity (velocity contrasts) or the traveltimes gradient (shocks). As a result, the computed amplitude either oscillates or changes its magnitude dramatically across those discontinuities. The same has been observed also for the ray-fan amplitudes by Dellinger et al. [1]; the large variations of the amplitude can introduce artifacts to the true-amplitude migration images.

This article is concerned with a concurrent simulation of the traveltimes and amplitude and introduces strategies for accurate FD approximations of the traveltimes derivatives. Essentially non-oscillatory (ENO) schemes [17] are adopted to sharply resolve discontinuities in the traveltimes and amplitude derivatives and to improve accuracy in smooth portions. See [2, 8, 9, 15, 16, 21] for applications of ENO schemes. For a full-aperture simulation, the combination of *down-n-out* (DNO) and the post-sweeping (PS) iteration is applied [5, 15]. The ENO scheme is also applied to the traveltimes second-derivatives in this article. Note that a complete derivation of the ENO scheme needs to incorporate a central approximation of the derivative under consideration. However, the central scheme for the traveltimes second-derivative in the amplitude-marching direction (e.g. τ_{zz} in the down-going marching) may not be obtained when utilizing the grid values, because the traveltimes values in the downwind direction are not available in a concurrent simulation of traveltimes and amplitudes. To overcome the difficulty, the derivative is approximated by simply incorporating the mid-step solution of the traveltimes.

To improve accuracy of the traveltimes and amplitude, in particular, in regions of large curvatures such as near the source, I introduce a new family of second-order difference method, called *quadratic ENO* (QENO) scheme which approximates the traveltimes derivatives *exactly* when the wavefront is circular or elliptical. An accurate approximation of the average slowness (which is different from the slowness smoothing) is considered for a better accuracy of the traveltimes. The resulting algorithm incorporating the new schemes and strategies turns out to show a second-order accuracy for the traveltimes and a first-order accuracy for the amplitude at points far away from the shocks.

An outline of the paper is as follows. The next section reviews the governing equations and considers difficulties in the amplitude computation. The following section presents ENO schemes for the traveltime second-derivatives. Then, the maximum angle condition is applied to the transport equation for the amplitude to be over-estimated for rays of large angles from the amplitude-marching direction; the over-estimation can be cured in the PS iteration by choosing the smaller value between the old and new solutions. The following section introduces QENO, extrapolation of the ENO approximation of the traveltime Laplacian, and an accurate approximation of the average slowness. Then, we present numerical results: comparisons of accuracy and efficiency between ENO and QENO, accuracy of amplitudes, and performance of the resulting algorithm for real velocity models. The last section includes conclusions. In Appendix A, we review the ENO eikonal solver along with the DNO-PS iteration.

2. Preliminaries

In this section, we present the governing equations for the traveltime and amplitude and discuss difficulties in the amplitude computation.

2.1. The governing equations

The traveltime and amplitude can be computed as the solutions of the *eikonal* and *transport* equations:

$$\begin{aligned} \text{(a)} \quad & |\nabla\tau|^2 = \frac{1}{v^2(\mathbf{x})}, \\ \text{(b)} \quad & 2\nabla\tau \cdot \nabla a + a\nabla^2\tau = 0, \end{aligned} \tag{2.1}$$

where $\tau = \tau(\mathbf{x}_s, \mathbf{x})$ is the traveltime function from the source \mathbf{x}_s to the location $\mathbf{x} = (x, y, z) = (x_1, x_2, x_3)$, $a = a(\mathbf{x}_s, \mathbf{x})$ is the amplitude, and v denotes the wavefront normal velocity. Let us introduce a convenient variable

$$u := \log\left(\frac{1}{a}\right) = -\log a, \tag{2.2}$$

which I call the *smallness*. Then, for e.g. down-going wavefronts, we can rewrite (2.1) as the following Hamilton-Jacobi differential equations

$$\begin{aligned} \text{(a)} \quad & \tau_z = H(\tau_x, \tau_y, \mathbf{x}), \\ \text{(b)} \quad & u_z = \Psi(u_x, u_y, \mathbf{x}), \end{aligned} \tag{2.3}$$

where

$$\begin{aligned} H(\tau_x, \tau_y, \mathbf{x}) &= \sqrt{s^2 - \tau_x^2 - \tau_y^2}, \\ \Psi(u_x, u_y, \mathbf{x}) &= \tau_z^{-1} \left(\frac{1}{2} \nabla^2 \tau - \tau_x u_x - \tau_y u_y \right). \end{aligned} \tag{2.4}$$

Here s ($:= 1/v$) is called the *slowness*.

The traveltime and smallness can be solved on regular meshes by applying second- or higher-order FD schemes to the eikonal and transport equations [3, 16, 19]. Since the transport equation incorporates the gradient and Laplacian of the traveltime, both the traveltime and its derivatives should be computed or approximated accurately for a reasonable accuracy of the smallness. See Appendix A for a second-order ENO eikonal solver.

2.2. Difficulties in the smallness computation

To get an accurate smallness, one may apply high-order difference schemes for both eikonal and transport equations, e.g., a third-order scheme for the eikonal equation and a second-order method for the transport equation. However, in real media, it is very hard to compute the smallness in a desired accuracy, due to discontinuities in the traveltime and velocity. Main technical difficulties can be summarized as follows:

- *Traveltime accuracy at caustics:* The ENO schemes [17, 18] have been widely utilized to sharply resolve discontinuities in the traveltime derivatives and to improve accuracy in smooth portions of the traveltime. See [2, 8, 9, 15, 16, 21]. Since one-sided high-order schemes can be unstable, a stable shock-capturing eikonal solver must be designed in such a way that the accuracy becomes lower-order (in practice, first-order) at caustics.
- *Accuracy of traveltime Laplacian:* The smallness is strongly affected by accuracy of the traveltime Laplacian. It has been known in conventional numerical analysis that the approximation of the traveltime Laplacian can show two-order lower accuracy than the traveltime itself. Thus, the traveltime seems to be computed by at least third-order methods to give a positive-order accuracy to the traveltime Laplacian; yet, since the traveltime has a first-order accuracy at caustics, a positive-order accuracy can hardly be observed for the traveltime Laplacian. As a matter of fact, naive approximations of the traveltime Laplacian can easily show a negative-order accuracy; near caustics, the error can increase as the mesh size decreases.
- *Concurrent simulation of the traveltime and smallness:* A concurrent simulation is desirable and challenging as well; first of all, the traveltime gradient utilized in the traveltime computation can be reused for the smallness computation. Furthermore, when one wants to compute the traveltime of the most-energetic wavefronts, the smallness must be available to decide the upwind direction of the traveltime; see [6, 10, 12]. However, there is a difficulty in the approximation of τ_{zz} (for the down-marching), because the approximation requires traveltime

values to be computed later. As a remedy, Symes and his colleagues [16, 21] rewrote τ_{zz} in a form involving only first z -derivatives:

$$\begin{aligned} \tau_{zz} = \tau_z^{-2} & \left[\frac{1}{2} \left(\tau_z(s^2)_z - \tau_x(s^2)_x - \tau_y(s^2)_y \right) \right. \\ & \left. + \tau_x^2 \tau_{xx} + \tau_y^2 \tau_{yy} + 2\tau_x \tau_y \tau_{xy} \right], \end{aligned} \quad (2.5)$$

which was obtained by differentiating the eikonal equation followed by some algebra. However, such a manipulation introduces a large error in general models where the slowness gradient is discontinuous.

3. ENO Schemes

In the traveltimes computation, upwind schemes are necessary to sharply resolve the discontinuities in the gradients, while central schemes are desired to improve accuracy. To satisfy the requirements, Kim and Cook [15] and Kim [8, 9] have employed a family of ENO schemes [17, 18] and numerically verified them to be particularly appropriate.

A rapidly varying traveltimes Laplacian can deteriorate the accuracy of ray-fan amplitudes [1]; the same has been observed for the FD smallness. That is, the same requirements for the traveltimes computation must be satisfied for the FD schemes for the traveltimes derivatives and smallness. Thus it seems natural to apply ENO schemes for all derivatives in the eikonal and transport equations (2.3).

When second-order difference schemes are carefully designed for the traveltimes and smallness derivatives, the traveltimes Laplacian (and therefore the smallness) can show a first-order accuracy in smooth portions [16]. Such an extra accuracy is called *superconvergence*. Here the main requirement for superconvergence is that the derivatives should be approximated by central schemes. However, the difference schemes must be upwind to accurately resolve the discontinuities in the traveltimes gradient, for which we would employ the second-order ENO scheme for the derivatives of the traveltimes and smallness. In this section, we focus on the ENO scheme for the traveltimes Laplacian: $\tau_{x_\ell x_\ell}$, $\ell = 1, 2$, and τ_{zz} for down-marching wavefronts.

3.1. ENO scheme for $\tau_{x_\ell x_\ell}$, $\ell = 1, 2$

The basic idea of the ENO scheme is to choose the least oscillatory component of the FD approximation among all possible differences satisfying a desired accuracy. I suggest an ENO scheme for τ_{xx} as follows. First, define difference operators

$$\begin{aligned} D_{xx}^- \tau_{ij}^k &= \min \left(L_{x,0} \tau_{ij}^k, L_{x,-1} \tau_{ij}^k \right), \\ D_{xx}^+ \tau_{ij}^k &= \min \left(L_{x,0} \tau_{ij}^k, L_{x,+1} \tau_{ij}^k \right), \end{aligned} \quad (3.1)$$

where, for $p = -1, 0, 1$,

$$L_{x,p}\tau_{ij}^k = \max\left(0, \frac{\tau_{i+p-1,j}^k - 2\tau_{i+p,j}^k + \tau_{i+p+1,j}^k}{(\Delta x)^2}\right). \quad (3.2)$$

Then, the ENO scheme for τ_{xx} can be formulated as

$$\widehat{D}_{xx}\tau_{ij}^k = \begin{cases} D_{xx}^-\tau_{ij}^k, & \text{if } \widehat{D}_x\tau_{ij}^k \geq 0, \\ D_{xx}^+\tau_{ij}^k, & \text{otherwise.} \end{cases} \quad (3.3)$$

The ENO scheme (3.3) clearly corresponds to the least oscillatory component of the traveltime Laplacian and its upwind direction matches with that of the traveltime. It shows a second-order accuracy when $L_{x,0}$ is selected, and a first-order accuracy otherwise. However, the scheme is *essentially second-order* in smooth models. To see this, consider wavefronts pointing at the $(x+)$ -direction in a linear model. The curvature of the wavefront is smaller as the wavefront marches, which guarantees $D_{xx}^-\tau_{ij}^k = L_{x,0}\tau_{ij}^k$, the second-order approximation of τ_{xx} at \mathbf{x}_{ij}^k . One can reach at the same conclusion for wavefronts propagating to the $(x-)$ -direction. Note that $\widehat{D}_{xx}\tau_{ij}^k = 0$ at shocks; more precisely, the scheme returns zero at all points where the wavefront is locally concave, which may be a drawback for some applications.

3.2. ENO scheme for τ_{zz} and mid-step traveltimes

For a simultaneous simulation of the traveltime and smallness e.g. for down-going wavefronts in (2.3), a challenging task is to design a central difference scheme (and a second-order ENO scheme) for τ_{zz} . A strategy is to compute the smallness at a level behind. That is, the smallness at the k -th depth level is computed after the traveltime computation at the $(k+1)$ -th level, which is not a real simultaneous simulation. In this subsection, we introduce a trick for the central difference scheme for τ_{zz} for a concurrent simulation of the traveltime and smallness.

Assume that the traveltime and smallness have been computed up to the k -th depth level, and the ENO schemes are to be applied to get the values on the $(k+1)$ -th level. As usual, we first carry out the computation for the traveltime and then for the smallness. The traveltime computation often requires a few marchings of a substep size Δz_{sub} , where $\Delta z = n_b \Delta z_{\text{sub}}$ for an integer $n_b \geq 1$. Here Δz_{sub} can be determined by incorporating the CFL stability condition, the maximum angle condition, or both. See the following section.

In Figure 1, the substeps are indicated with the dashed lines. One may set the number of substeps even, i.e. $n_b = 2m$ for some m . The mid-step traveltime $\tau^{k+1/2}$ can be saved into a temporary memory right after carrying out the m -th substep.

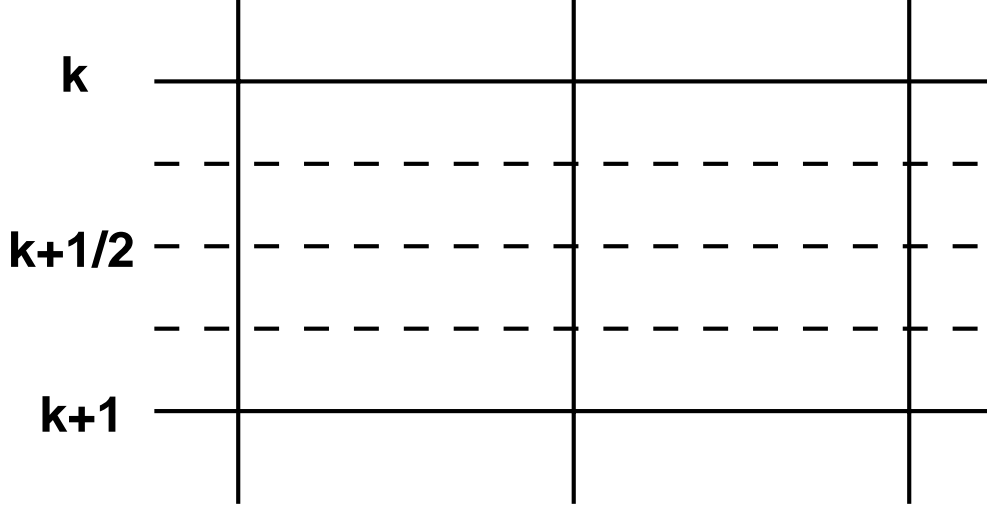


Figure 1: The mid-step solution $\tau^{k+1/2}$ in the traveltime computation.

After finishing the traveltime computation for the $(k + 1)$ -th depth level, one can compute

$$L_{z,1/2}\tau_{ij}^k := \max\left(0, \frac{\tau_{ij}^k - 2\tau_{ij}^{k+1/2} + \tau_{ij}^{k+1}}{(\Delta z/2)^2}\right), \quad (3.4)$$

with which the second-order ENO scheme for τ_{zz} for down-going wavefronts can be formulated as

$$\widehat{D}_{zz}\tau_{ij}^{k+1/2} = \min\left(L_{z,0}\tau_{ij}^k, L_{z,1/2}\tau_{ij}^k\right), \quad (3.5)$$

where

$$L_{z,0}\tau_{ij}^k := \max\left(0, \frac{\tau_{ij}^{k-1} - 2\tau_{ij}^k + \tau_{ij}^{k+1}}{(\Delta z)^2}\right). \quad (3.6)$$

Here $L_{z,1/2}\tau_{ij}^k$ and $L_{z,0}\tau_{ij}^k$ serve as the central and one-sided differences, respectively.

Remark. In the smallness computation between the k -th and the $(k + 1)$ -th depth planes, it is reasonable to utilize the mid-step traveltime $\tau^{k+1/2}$ for all traveltime derivatives appeared in the transport equation in (2.3). Explicitly, we approximate

$$(\tau_{x_\ell})_{ij}^{k+1/2} \approx \widehat{D}_{x_\ell}\tau_{ij}^{k+1/2}, \quad \ell = 1, 2, \quad (3.7)$$

where \widehat{D}_{x_ℓ} is defined in (A.4). An ENO scheme for τ_z on $\{(x, y, z) : z \in [z^k, z^{k+1}]\}$ can be formulated by checking if

$$\tau_{ij}^{k-1} - 2\tau_{ij}^k + \tau_{ij}^{k+1} \geq 4(\tau_{ij}^k - 2\tau_{ij}^{k+1/2} + \tau_{ij}^{k+1}); \quad (3.8)$$

I suggest the ENO scheme for τ_z as follows:

$$\begin{aligned}
 (\tau_z)_{ij}^{k+1/2} &\approx (\tau_{x_z})_{ij}^{k+1/2} \\
 &:= \begin{cases} \frac{\tau_{ij}^{k+1} - \tau_{ij}^k}{\Delta z}, & \text{if (3.8) is satisfied,} \\ \frac{\tau_{ij}^{k-1} - 9\tau_{ij}^k + 8\tau_{ij}^{k+1/2}}{3\Delta z}, & \text{else,} \end{cases} \quad (3.9)
 \end{aligned}$$

which approximates τ_z at the mid-step ($\mathbf{x} = \mathbf{x}_{ij}^{k+1/2}$), corresponding to (3.5).

4. Maximum Angle Condition

There is no limitation for the iteration DNO-PS to be applied to the smallness computation when incorporated with a proper *maximum angle condition* (MAC). MAC is first introduced by Gray and May [4] to accurately compute traveltimes along the rays whose velocity vectors make angle to the vertical not larger than a prescribed angle θ_{\max} [15, 16, 19]. MAC has been further explored as a tool for an over-estimation of the traveltime when the FD marching is unstable numerically, more precisely, when the ray angle is larger than θ_{\max} measured from the ENO marching direction [8, 15]. Since other directional marchings are to be applied during the PS iteration, the accuracy of traveltimes for the large-angle rays can be momentarily ignored provided that the unstable traveltimes are over-estimated. Note that the PS iteration is introduced to cure the instability by eliminating the over-estimated traveltimes.

To introduce a MAC for the smallness computation, it is instructive to consider the MAC for the traveltime computation. Consider rays whose velocity vectors make angle θ with the vertical not larger than θ_{\max} :

$$|\sin \theta| \leq \sin \theta_{\max} < 1. \quad (4.1)$$

To enforce this condition, we modify the eikonal equation (2.3.a). Note that

$$\sin^2 \theta = \frac{\tau_x^2 + \tau_y^2}{|\nabla \tau|^2} = \frac{\tau_x^2 + \tau_y^2}{s^2}, \quad (4.2)$$

and therefore

$$\tau_z^2 = s^2 - \tau_x^2 - \tau_y^2 = s^2 - s^2 \sin^2 \theta = s^2 \cos^2 \theta. \quad (4.3)$$

The condition (4.1) turns out to be

$$\tau_z \geq s \cdot \cos \theta_{\max}, \quad 0 < \theta_{\max} < \frac{\pi}{2}. \quad (4.4)$$

Therefore, the eikonal equation (2.3.a) incorporating MAC reads

$$\tau_z = \sqrt{\max(s^2 \cos^2 \theta_{\max}, s^2 - \tau_x^2 - \tau_y^2)}. \quad (4.5)$$

The same strategy can be applied to the smallness computation, assuming the propagation direction of τ is the same as that of the smallness. Here the difference is that $\frac{1}{2}\nabla^2\tau$ plays the role of s^2 . A MAC-enforced transport equation for the down-going smallness can be formulated as follows:

$$u_z = \tau_z^{-1} \max\left(\frac{1}{2}\nabla^2\tau \cdot \cos \theta_{\max}, \frac{1}{2}\nabla^2\tau - \tau_x u_x - \tau_y u_y\right). \quad (4.6)$$

Note that the ENO schemes (3.3) and (3.5) produce nonnegative values for the components of the traveltime Laplacian. It is recommended to choose θ_{\max} corresponding to 2 or 4 substeps, i.e., $\cos \theta_{\max} = 1/(1 + n_b^2)^{1/2}$, where n_b is 2 or 4.

Remark. MACs in (4.5) and (4.6) can be combined with the CFL stability condition for an efficient computation. It is occasionally true that the ray directions in a given directional marching are not so much diverse that the computation on the given step can be carried out by a smaller number of substeps than the prescribed one. In the case, the traveltime can be computed more efficiently incorporating the CFL condition [15]:

$$\Delta z_{\text{sub}} \leq \min_{i,j} \left[\frac{H[\tau]_{i,j}^k}{\sqrt{(\widehat{D}_x^2 \tau_{i,j}^k)^2 + (\widehat{D}_y^2 \tau_{i,j}^k)^2}} \right] \cdot \frac{\Delta x \Delta y}{\sqrt{\Delta x^2 + \Delta y^2}}. \quad (4.7)$$

That is, the number of substeps can be chosen as the minimum between the prescribed one (enforcing the MAC) and the one from the CFL condition. However, the substep number must be adjusted to be even, to save the mid-step solution required for the smallness computation.

5. Accuracy Improvement

In this section, we consider extra strategies to further improve accuracy of the traveltime and smallness.

5.1. Quadratic ENO

It is occasionally the case that the wavefronts look *locally* circular or elliptical. It is particularly true when the velocity is locally linear. To take an advantage of the observation, we begin with the traveltime in a constant velocity v_0 :

$$\tau^2(\mathbf{x}_s, \mathbf{x}) = \frac{1}{v_0^2} |\mathbf{x} - \mathbf{x}_s|^2, \quad (5.1)$$

which is a quadratic polynomial in the variables (x, y, z) . The squared traveltime τ^2 is in general quadratic for circular or elliptical wavefronts.

Assume that τ^2 is locally quadratic. Then, all second-order FD schemes applied for $\nabla(\tau^2)$ and $\Delta(\tau^2)$ in smooth portions would be exact! Note that for $\ell, m = 1, 2, 3$,

$$\begin{aligned}\tau_{x_\ell} &= \frac{1}{2\tau} (\tau^2)_{x_\ell} \\ \tau_{x_\ell x_m} &= \frac{1}{2\tau} [(\tau^2)_{x_\ell x_m} - 2\tau_{x_\ell} \tau_{x_m}].\end{aligned}\tag{5.2}$$

So, if \widehat{D}_{x_ℓ} and $\widehat{D}_{x_\ell x_m}$ are second-order (central) approximations of ∂_{x_ℓ} and $\partial_{x_\ell x_m}$, respectively, then the following schemes are exact:

$$\begin{aligned}(\tau_{x_\ell})_{ij}^k &\approx \widetilde{D}_{x_\ell} \tau_{ij}^k := \frac{1}{2\tau_{ij}^k} \widehat{D}_{x_\ell} (\tau^2)_{ij}^k, \\ (\tau_{x_\ell x_m})_{ij}^k &\approx \widetilde{D}_{x_\ell x_m} \tau_{ij}^k \\ &:= \frac{1}{2\tau_{ij}^k} \left(\widehat{D}_{x_\ell x_m} (\tau^2)_{ij}^k - \widetilde{D}_{x_\ell} \tau_{ij}^k \cdot \widetilde{D}_{x_m} \tau_{ij}^k \right).\end{aligned}\tag{5.3}$$

However, in practice, the FD schemes cannot be central where shocks develop. We call the above approximations the *quadratic ENO* (QENO) schemes when the differences \widehat{D}_{x_ℓ} and $\widehat{D}_{x_\ell x_m}$ are replaced by ENO schemes defined in (A.4), (3.3), (3.5), and (3.9); ENO-RK2 (A.5) incorporating (5.3) will be called *QENO-RK2*. Although the difference schemes in the pseudo-spatial directions are exact for elliptical wavefronts, QENO-RK2 may not be exact due to the conventional approximation in the pseudo-temporal (marching) direction. Due to a heavier incorporation of the square operations, QENO-RK2 is about 50% more expensive than ENO-RK2 for problems of the same size.

QENO was originally introduced to accurately approximate the traveltime near the source [13, 14]. It has been applied to the computation of traveltimes and smallness and the traveltime interpolation in various velocity models; QENO shows an excellent accuracy for the interpolated traveltimes but it turns out to be sensitive to the traveltime error in the traveltime/smallness computation [14]. It is not recommended to be utilized for the traveltime/smallness computation in oscillatory media. Superiority of QENO is presented later in this article, when applied to the traveltime computation in smooth models.

5.2. Extrapolation of $\nabla^2 \tau$ at artificial shocks

For a full-aperture simulation of the traveltime and smallness, we have adopted the iteration strategy: DNO-PS [5, 15]. See Appendix A. In the DNO step, the edges of the down- and out-facing planes serve as a sort of *artificial* shocks, because the

ENO schemes must be one-sided at grid points on those edges. Since accuracy of the traveltime is deteriorated to become first-order at shocks (physical or artificial), ENO approximations of the traveltime Laplacian, and therefore the smallness, may show a relatively large error on the edges.

To avoid such a undesirable accuracy degradation, we introduce the following extrapolation scheme at the artificial shocks in the DNO step: For the wavefront moving forward, for example,

$$(\tau_{xx})_{ij}^k \approx E(\widehat{D}_{xx}\tau_{ij}^k) := 2\widehat{D}_{xx}\tau_{i-1,j}^k - \widehat{D}_{xx}\tau_{i-2,j}^k, \quad (5.4)$$

where $\widehat{D}_{xx}\tau_{ij}^k$ is defined in (3.3). The same strategy can be adopted for other directional derivatives, τ_{yy} and τ_{zz} , to be approximated at the artificial shocks. Note that when both $\widehat{D}_{xx}\tau_{i-1,j}^k$ and $\widehat{D}_{xx}\tau_{i-2,j}^k$ are chosen to be central, the extrapolation $E(\widehat{D}_{xx}\tau_{ij}^k)$ is an one-sided second-order difference approximation of τ_{xx} at $\mathbf{x} = \mathbf{x}_{ij}^k$.

Remark. The extrapolation scheme (5.4) can be utilized at the physical shocks as well. More precisely, apply (5.4) when

$$D_x^- D_x^+ \tau_{ij}^k < 0, \quad \min(D_x^- D_x^- \tau_{ij}^k, D_x^+ D_x^+ \tau_{ij}^k) > 0. \quad (5.5)$$

However, no apparent accuracy improvement has been observed for the modification.

5.3. Average slowness

For e.g. the down-going ENO marching, the average slowness can be accurately approximated by averaging the slowness along the vertical line segment $\overline{\mathbf{x}_{ij}^k \mathbf{x}_{ij}^{k+1}}$, where $\mathbf{x}_{ij}^{k+1} = \mathbf{x}_{ij}^k + (0, 0, \Delta z)$ [15]. More accurate average slowness can be computed by incorporating information of the wavefront normal as follows. Let θ_x and θ_y be the angles of x - and y -components of $\nabla\tau_{i,j}^k$ from the vertical, respectively. Consider

$$\mathbf{x}_{i,j}^{\sigma,k} = \mathbf{x}_{i,j}^k + \sigma \cdot \Delta z (\tan\theta_x, \tan\theta_y, 0), \quad (5.6)$$

where $\sigma \in [0, 1]$ is a regularization parameter and

$$\begin{aligned} \tan\theta_x &\approx \widehat{D}_y\tau_{i,j}^k / \left((s_{i,j}^k)^2 - (\widehat{D}_x\tau_{i,j}^k)^2 \right)^{1/2}, \\ \tan\theta_y &\approx \widehat{D}_x\tau_{i,j}^k / \left((s_{i,j}^k)^2 - (\widehat{D}_y\tau_{i,j}^k)^2 \right)^{1/2}. \end{aligned} \quad (5.7)$$

When $\sigma = 1$, $\mathbf{x}_{i,j}^{\sigma,k}$ approximates the point from which a ray comes out to reach at $\mathbf{x}_{i,j}^{k+1}$ first; one has to set $\sigma \cong 1/n_b$ for the traveltime computation with n_b substeps.

Thus, with σ suitably chosen, one can obtain an accurate average slowness

$$\begin{aligned} \widehat{s}_{i,j}^{\sigma,k} &:= \frac{1}{|\mathbf{x}_{i,j}^{k+1} - \mathbf{x}_{i,j}^{\sigma,k}|} \cdot \int_{\mathbf{x}_{i,j}^{\sigma,k}}^{\mathbf{x}_{i,j}^{k+1}} \frac{1}{v(\mathbf{x}')} d\gamma \\ &= \begin{cases} 1/v_{i,j}^{\sigma,k}, & \text{if } v_{i,j}^{k+1} = v_{i,j}^{\sigma,k}, \\ \frac{\log(v_{i,j}^{k+1}/v_{i,j}^{\sigma,k})}{v_{i,j}^{k+1} - v_{i,j}^{\sigma,k}}, & \text{else,} \end{cases} \end{aligned} \quad (5.8)$$

where we have utilized the multi-linear profile of the velocity (given at grid points) and $v_{i,j}^{\sigma,k} = v(\mathbf{x}_{i,j}^{\sigma,k})$ is an interpolated velocity obtained incorporating adjacent four values in the k -th level. For other directional marching, one can get the average slowness in a similar way.

It should be noticed that the slowness averaging is carried out inside the cell and that the velocity values given on grid points are never altered during the averaging. Such a slowness averaging is different from the *velocity smoothing* where the velocity values are reevaluated to satisfy certain smoothness criteria.

6. Numerical Experiments

In previous sections, I have introduced new difference schemes and strategies for an accurate simulation of the traveltimes and slowness. The main goal of this section is to verify them numerically for 3D velocity models.

6.1. Algorithm summary and implementation

First, we summarize the strategies and choices for an efficient implementation for a concurrent simulation of the traveltimes and slowness:

- The overall marching algorithm is ENO-DNO-PS [5, 15], applying (A.5) in various directions, for both traveltimes and slowness.
- The eikonal and transport equations are modified to incorporate MACs as in (4.5) and (4.6). MAC allows the algorithm to update the solutions iteratively by choosing the smaller value between the new and old solutions.
- The CFL condition (4.7) is integrated with MACs for a better efficiency.
- A cache-based implementation [8] is practiced to reduce the memory-access time, for the computation of both traveltimes and slowness.
- All derivatives in the pseudo-spatial directions (e.g., x - and y -directions in the down-going marching) are approximated by the second-order ENO scheme.

Table 1: Accuracy and efficiency of (A.5) for the traveltime computation in $v = v_1$.

	Δz_{sub}	$h = 200$		$h = 100$	
		$E_\infty[\tau]$	CPU	$E_\infty[\tau]$	CPU
ENO	50	3.08e-3	0.16	6.07e-4	0.66
	25	3.06e-3	0.31	5.92e-4	1.22
QENO	50	4.22e-5	0.23	4.01e-5	0.97
	25	1.16e-5	0.46	1.21e-5	1.84

- All traveltime derivatives in the transport equation are discretized incorporating the mid-step traveltime solutions, which makes the algorithm compute the traveltime and smallness accurately and concurrently.
- The ENO schemes for the traveltime second-derivatives are extrapolated near the artificial shocks in the DNO step, as suggested in (5.4).
- It has been numerically verified that the average slowness obtained from (5.6) and (5.8) with $\sigma = 0$ is accurate enough, efficient, and easy to implement.
- For real models, QENO-RK2 is applied to only the traveltime computation near the source, not larger than 16 grid lengths from the source. In heterogeneous models, no apparent accuracy improvement has been observed for QENO traveltimes.

The routines are written in FORTRAN; the computations are carried out on a 400MHz Laptop of a Linux operating system.

6.2. Accuracy analysis

In this subsection, we verify the superiority of QENO and accuracy of the smallness in smooth models. Let the computational domain be $(0, 6000 \text{ m})^3$. Choose two different smooth velocity models:

$$\begin{aligned} v_1(\mathbf{x}) &= 2000 \text{ m/s}, \\ v_2(\mathbf{x}) &= 1000 + 0.2x + 0.1y + 0.5z \text{ m/s}, \end{aligned} \tag{6.1}$$

and locate a point source at $\mathbf{x}_s = (3000, 3000, 0)$. Below CPU is measured in second for the user time and the error $E_\infty[\tau]$ is defined by

$$E_\infty[\tau] = \|\tau_{\text{comput}} - \tau_{\text{analytic}}\|_\infty, \tag{6.2}$$

where $\|\cdot\|_\infty$ denotes the maximum norm.

Table 2: Accuracy and efficiency of (A.5) for the traveltime computation in $v = v_2$.

	Δz_{sub}	$h = 200$		$h = 100$	
		$E_\infty[\tau]$	CPU	$E_\infty[\tau]$	CPU
ENO	50	3.63e-3	0.17	8.81e-4	0.77
	25	3.57e-3	0.32	8.78e-4	1.33
QENO	50	9.72e-4	0.25	4.10e-4	1.06
	25	9.28e-4	0.46	2.49e-4	1.90

In Table 1, we compare accuracy and efficiency of (A.5) between ENO and QENO for the traveltime computation in the constant velocity v_1 . Set $h = \Delta x = \Delta y = \Delta z$; in the DNO marching, a few substeps are applied in the pseudo-temporal (marching) directions. Accuracy of ENO is not improved for the smaller Δz_{sub} , because the errors in the x - and y -directions are clearly dominating the total error. On the other hand, QENO shows *little* sensitivity to the mesh refinement in the the x - and y -directions, which implies that the errors in the pseudo-spatial directions are *zero*. Overall, QENO dramatically improves the traveltime accuracy in the constant velocity for approximately 50 percent of extra cost.

Table 2 compares accuracy and efficiency, as in Table 1, for $v = v_2$. The algorithm incorporating ENO has produced the results as expected. As one can see from the table, QENO shows 3.5 to 4 times better accuracy than ENO in approximating the traveltime derivatives in the pseudo-spatial directions. It again requires about 50% extra computational cost.

Figure 2 depicts the smallness on a vertical section $\{y = 3000 \text{ m}\}$ for the constant velocity $v = v_1$. The mesh size $h = 100 \text{ m}$ and the substep size in the marching direction is automatically determined from the CFL condition (4.7) with $n_b \leq 4$, an enforcement of MAC. The traveltime is computed applying QENO near the source only, not larger than 16 grid lengths from the source. At the artificial shocks (the interfaces of the down and out marchings), the extrapolation scheme (5.4) is applied for the approximation of the traveltime Laplacian. The extrapolation gives an improved accuracy, but the computed smallness still exhibits an apparent error. The maximum error measured from the true smallness, $\log r$, $r = |\mathbf{x} - \mathbf{x}_s|$, turns out to be 0.048 which is approximately 0.5%. The error is measured for various grid sizes; the error near the artificial shocks does *not* decrease as the grid size becomes smaller, but remains under 1%. As shown in [16], the smallness shows a first-order accuracy in smooth regions.

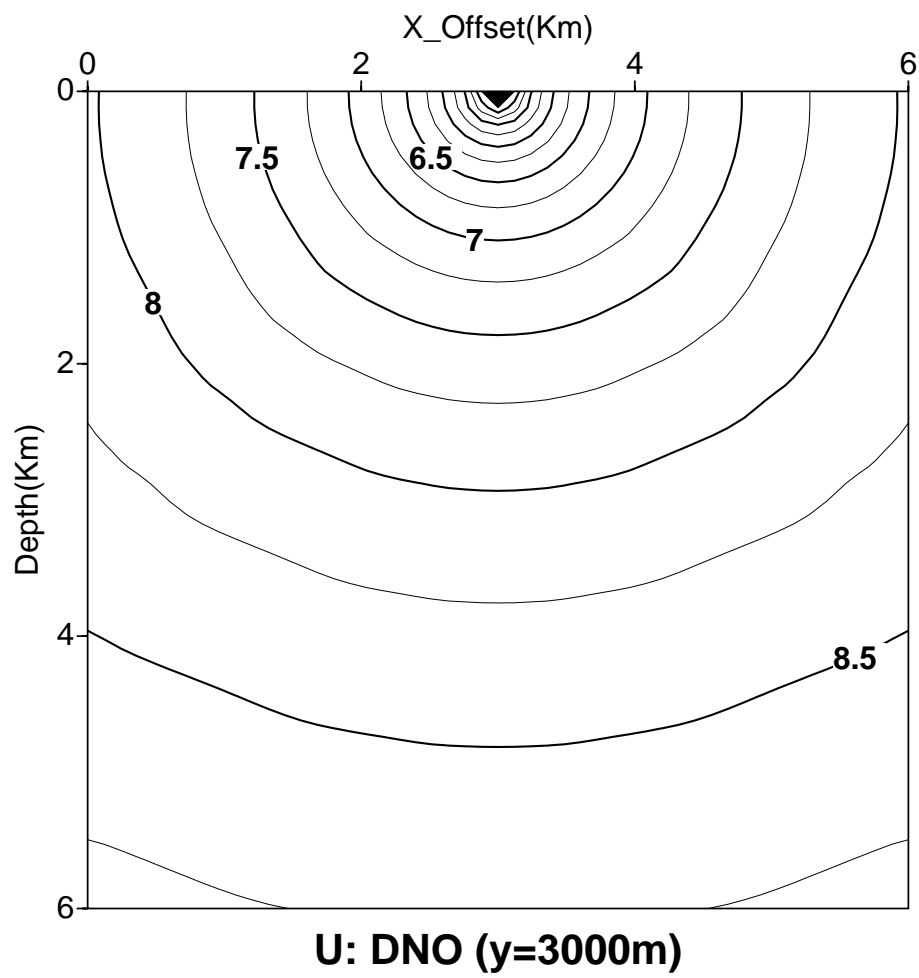


Figure 2: The smallness on a vertical section $\{y = 3000 \text{ m}\}$ for $v = v_1$.

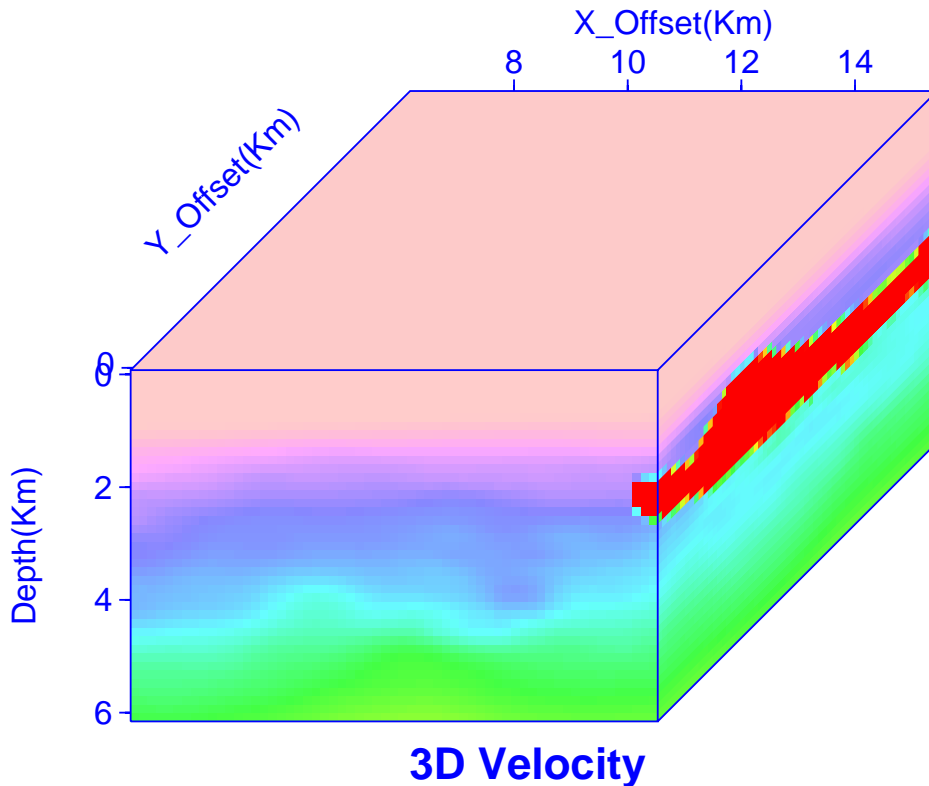
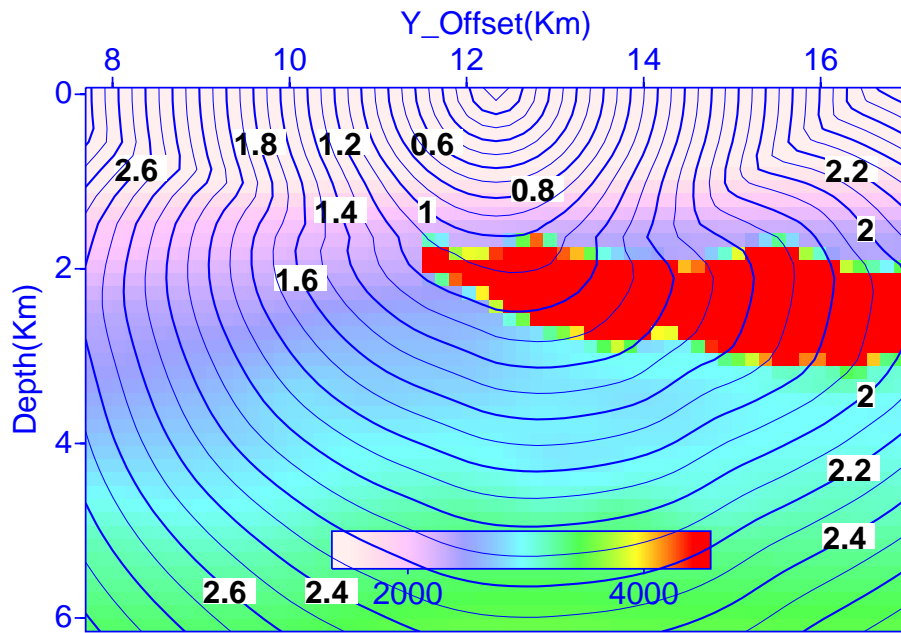


Figure 3: A velocity cube of $61 \times 61 \times 41$ cells in the Gulf of Mexico.

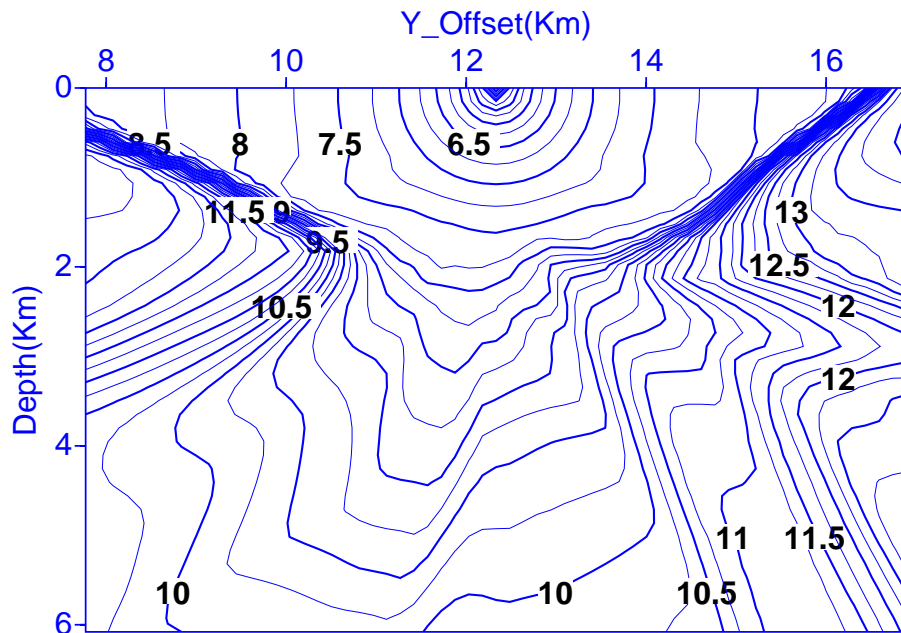
6.3. Smallness computation in real models

Now, we consider a real velocity cube of $61 \times 61 \times 41$ cells in the Gulf of Mexico, provided by Shell Offshore Inc.. See Fig. 3. The cell size is given 500^3 feet³ ($\cong 152.4^3 m^3$). A point source is located at $\mathbf{x}_s = (10858.5, 12344.4, 2.0)$ for a concurrent simulation of the traveltimes and smallness. The algorithm converges in two PS iterations for the stopping criterion of one millisecond, taking 6.5 seconds for the whole computation. Note that the number of cells in the velocity cube is 152,561. Since ENO-DNO-PS requires $\mathcal{O}(N)$ operations, where N is the number of grid points, the algorithm will take approximately 43 seconds on a 400MHz machine for the concurrent simulation of the traveltimes and smallness on one million cells.

Figures 4 and 5 present the computed results on the vertical sections $\{x = 10820\}$ and $\{y = 12340\}$, respectively; in each figure, the top depicts the computed traveltimes superposed on the velocity, while the bottom is the corresponding smallness. As one can see from the figures, the smallness is resolved quite reasonably, although the

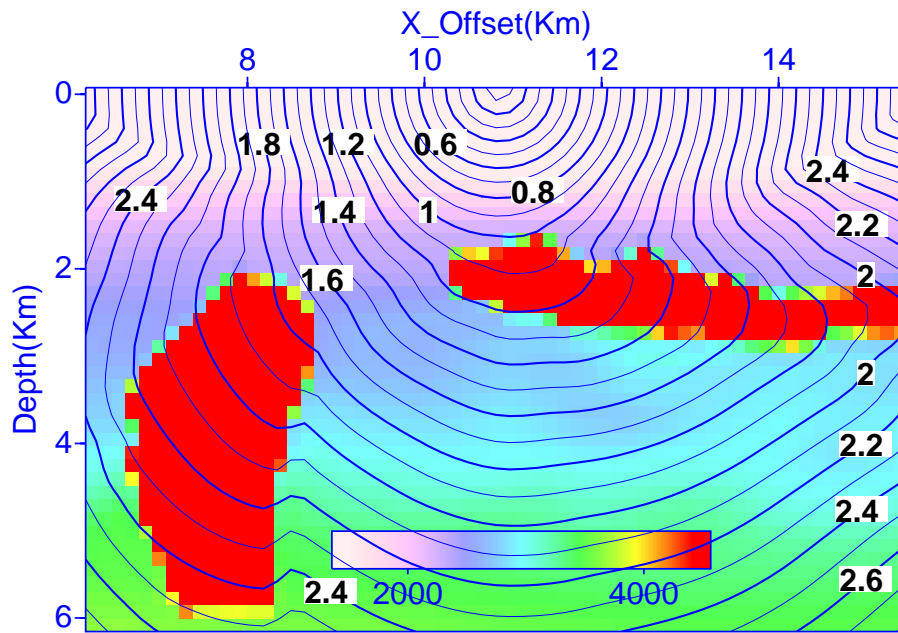


Velocity & TT (x=10820m)

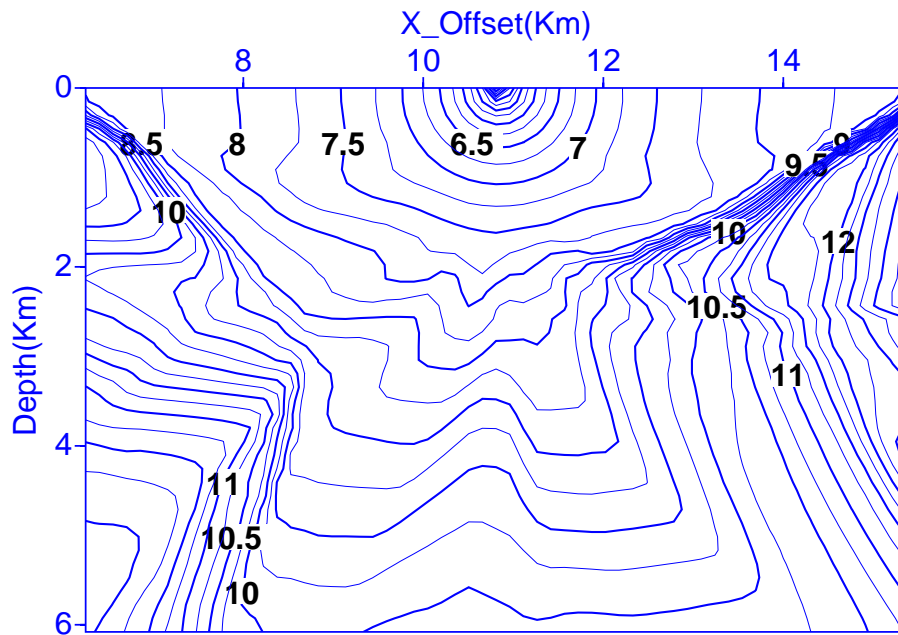


U: ENO-DNO-PS (x=10820m)

Figure 4: The computed traveltime superposed on the velocity on a vertical section $\{x = 10820\}$ (top) and the corresponding smallness (bottom).



Velocity & TT (y=12344m)



U: ENO-DNO-PS (y=12344m)

Figure 5: The computed traveltime superposed on the velocity on a vertical section $\{y = 12340\}$ (top) and the corresponding smallness (bottom).

grid size is as large as 152.4 m. To see more details, we will first focus on Figure 4. The computed traveltime in the figure shows a large curvature around the horizontal line $\{z = 2000 \text{ m}\}$; the smallness increases sharply toward the upwind ray directions. Notice that the traveltime is smooth and of small curvatures in the left-bottom portion of the figure, where the smallness increases relatively slowly. (This implies that the amplitude decreases slowly.) In general, the following has been observed: For the regions where the smallness increases more rapidly than the neighborhood (i.e., the smallness contours become locally concave toward the upwind ray direction), there correspond local maxima of the traveltime curvature, which is exactly what we have hoped and expected. One can make similar observations from Figure 5.

7. Conclusions

We have considered difference schemes and strategies for a simultaneous simulation of the traveltime and smallness by solving the eikonal and transport equations on regular grids. Second-order ENO schemes have been introduced for the traveltime second-derivatives to compute the smallness accurately and smoothly. A maximum angle condition is enforced for the smallness to be over-estimated when velocity vectors make large angles from the algorithm-marching direction and the post-sweeping iteration is imposed to cure the over-estimation efficiently. To improve traveltime accuracy near the source, we have introduced a new second-order ENO method, called the *quadratic ENO* (QENO) scheme which is exact for the traveltime derivatives when τ^2 can be expressed as a quadratic polynomial, i.e., the wavefront is circular or elliptical. An accurate approximation of the average slowness is considered to further improve the accuracy of the traveltime and therefore the smallness. The overall algorithm incorporating these new techniques turns out to be second-order accurate for the traveltime and first-order accurate for the smallness in smooth regions. The algorithm has been successfully tested for the traveltime-smallness computation in real velocity models of large contrasts. The computation of the most-energetic traveltime is the subject for the subsequent article [10].

Acknowledgment

The author wants to express his sincere thanks to Prof. W.W. Symes, Rice University, and Dr. R. Cook, Shell E&P Technology Co., for their interests, helpful comments, and encouragement. He deeply appreciates research management of Shell Offshore Inc. for allowing him to use a real model and publish related results.

References

- [1] J. DELLINGER, S. GRAY, G. MURPHY, J. ETGEN, AND T. FEI, *Efficient two and one-half dimensional true-amplitude migration*, in Expanded Abstracts, Society of Exploration Geophysicists, 1999, pp. 1540–1543.
- [2] J. DELLINGER AND W. W. SYMES, *Anisotropic finite-difference traveltimes using a Hamilton-Jacobi solver*, in Expanded Abstracts, Society of Exploration Geophysicists, 1997, pp. 1786–1789.
- [3] M. A. EL-MAGEED, *3D first arrival traveltimes and amplitudes via Eikonal and Transport finite difference solvers*, Ph.D. Thesis, Department of Computational and Applied Mathematics, Rice University, 6100 Main St., Houston Texas 77005, USA, 1996.
- [4] S. GRAY AND W. MAY, *Kirchhoff migration using eikonal equation traveltimes*, *Geophysics*, 59 (1994), pp. 810–817.
- [5] S. KIM, *ENO-DNO-PS: a stable, second-order accuracy eikonal solver*, in Expanded Abstracts, Tulsa, OK, 1999, Society of Exploration Geophysicists, pp. 1747–1750.
- [6] —, *On most-energetic traveltimes*, in Expanded Abstracts, Tulsa, OK, 2000, Society of Exploration Geophysicists, pp. 946–949.
- [7] —, *Wavefronts of linear elastic waves: local convexity and modeling*, *Wave Motion*, 32 (2000), pp. 203–216.
- [8] —, *3D eikonal solvers, Part I: First-arrival traveltimes*, *Geophysics*, (2001). (to appear).
- [9] —, *3D eikonal solvers, Part II: Anisotropic traveltimes*, *Geophysics*, (2001). (to appear).
- [10] —, *3D eikonal solvers, Part IV: Most-energetic traveltimes*. (in preparation), 2001.
- [11] —, *An $\mathcal{O}(N)$ level set method for eikonal equations*, *SIAM J. Sci. Comput.*, 22 (2001), pp. 2178–2193.
- [12] —, *The most-energetic traveltime of seismic waves*, *Appl. Math. Letters*, 14 (2001), pp. 313–319.

- [13] —, *On accuracy and efficiency of eikonal solvers*. (preprint), 2001.
- [14] —, *On accuracy of finite difference amplitudes and interpolated traveltimes*, in Expanded Abstracts, Tulsa, OK, 2001, Society of Exploration Geophysicists, pp. 1175–1178.
- [15] S. KIM AND R. COOK, *3D traveltime computation using second-order ENO scheme*, *Geophysics*, 64 (1999), pp. 1867–1876.
- [16] S. KIM, W. SYMES, AND M. A. EL-MAGEED, *Superconvergent difference formulas for traveltimes and amplitudes*, in *Mathematical and Numerical Aspects of Wave Propagation*, J. A. DeSanto, ed., Philadelphia, 1998, SIAM, pp. 591–593.
- [17] S. OSHER AND J. SETHIAN, *Fronts propagating with curvature dependent speed: algorithms based on Hamilton-Jacobi formulations*, *J. Comp. Phys.*, 79 (1988), pp. 12–49.
- [18] S. OSHER AND C.-W. SHU, *High-order essentially nonoscillatory schemes for Hamilton-Jacobi equations*, *SIAM J. Numer. Anal.*, 28 (1991), pp. 907–922.
- [19] J. QIAN, C. BELFI, AND W. SYMES, *Adaptive finite-difference method for traveltime and amplitude*, in Expanded Abstracts, Tulsa, OK, 1999, Society of Exploration Geophysicists, pp. 1763–1766.
- [20] J. SETHIAN, *A fast marching level set method for monotonically advancing fronts*, *Proc. Natl. Acad. Sci. USA*, 93 (1996), pp. 1591–1595.
- [21] W. W. SYMES, R. VERSTEEG, A. SEI, AND Q.-H. TRAN, *Kirchhoff simulation migration and inversion using finite-difference traveltimes and amplitudes*, TRIP Annual Report, The Rice Inversion Project, Rice University, Houston, TX 77005, 1994.
- [22] J. TSITSIKLIS, *Efficient algorithms for globally optimal trajectories*, *IEEE Transactions on Automatic Control*, 40(9) (1995), pp. 1528–1538.
- [23] J. E. VIDALE, *Finite-difference calculation of travel times*, *Bull., Seis. Soc. Am.*, 78 (1988), pp. 2062–2076.
- [24] —, *Finite difference calculation of traveltimes in three dimensions*, *Geophysics*, 55 (1990), pp. 521–526.

A. Eikonal Solver

For a completeness of the article, here we review a second-order algorithm for the eikonal equation which is easily applicable to the transport equation.

A.1. Second-order ENO eikonal solver

For the shock-capturing finite difference scheme of second-order accuracy, we choose the *essentially non-oscillatory* (ENO) schemes [17, 18] as particularly appropriate; see [5, 15]. This subsection presents the second-order eikonal solver incorporating the ENO scheme of Osher and Sethian [17]. Let's begin with defining the forward (+) and backward (−) finite difference operators:

$$D_x^\pm \tau_{i,j}^k = \pm \frac{\tau_{i\pm 1,j}^k - \tau_{i,j}^k}{\Delta x}, \quad (\text{A.1})$$

where i , j , and k are respectively x , y , and z indices, with $\tau_{ij}^k = \tau(\mathbf{x}_s, \mathbf{x}_{ij}^k)$. Then, the second-order ENO differences for τ_x read

$$\tau_x \approx D_x^{\pm,2} \tau := D_x^\pm \tau \mp \frac{1}{2} \Delta x \cdot m(D_x^- D_x^+ \tau, D_x^\pm D_x^\pm \tau), \quad (\text{A.2})$$

where

$$m(a, b) = \begin{cases} 0, & \text{if } ab \leq 0, \\ a, & \text{if } |a| \leq |b| \text{ and } ab > 0, \\ b, & \text{if } |a| > |b| \text{ and } ab > 0. \end{cases} \quad (\text{A.3})$$

Now, define the second-order *upwind* ENO approximation for τ_x incorporating the first-arrivals:

$$(\tau_x)_{i,j}^k \approx \widehat{D}_x \tau_{i,j}^k := \text{mod_max}(\max(D_x^{-,2} \tau_{i,j}^k, 0), \min(D_x^{+,2} \tau_{i,j}^k, 0)), \quad (\text{A.4})$$

where “mod_max” returns the larger value in modulus. Defining the analogue $\widehat{D}_y \tau_{i,j}^k$ for τ_y , we formulate the second-order, upwind, ENO Runge-Kutta (ENO-RK2) algorithm as follows:

$$\begin{aligned} \tau_{i,j}^{k+\frac{1}{2}} &= \tau_{i,j}^k + \Delta z_{\text{sub}} \cdot H[\tau]_{i,j}^k, \\ \tau_{i,j}^{k+1} &= \frac{1}{2} \left(\tau_{i,j}^k + \tau_{i,j}^{k+\frac{1}{2}} + \Delta z_{\text{sub}} \cdot H[\tau]_{i,j}^{k+\frac{1}{2}} \right), \end{aligned} \quad (\text{A.5})$$

where

$$H[\tau]_{i,j}^k = \sqrt{(s_{i,j}^k)^2 - (\widehat{D}_x \tau_{i,j}^k)^2 - (\widehat{D}_y \tau_{i,j}^k)^2}. \quad (\text{A.6})$$

Here Δz_{sub} is to be determined by the CFL condition and/or a maximum angle condition. Since the velocity model is often provided in a uniform mesh of the cell size $(\Delta x, \Delta y, \Delta z)$, a certain number of substeps (of size Δz_{sub}) should be imposed

in a step (of size Δz) to satisfy the CFL/maximum-angle condition. That is, the traveltimes computation for a cell layer should be performed by marching several substeps of size Δz_{sub} . The incorporation of substeps is also an essential ingredient for a fast convergence of iterative eikonal solvers [13].

It has been observed from various numerical experiments that $\widehat{D}_x \tau$ is mostly-centered and sharply resolves shocks. Hence, the algorithm is of *mostly* second-order accuracy [5, 15]. After carrying out the traveltimes computation from the k -th level to the next, ENO-RK2 can be applied to the transport equation by replacing τ and H respectively by u and Ψ , provided that ENO approximations for all derivatives in the Hamiltonian Ψ are available.

A.2. DNO-PS: the iteration strategy

To achieve a high-order accuracy in realistic media, the ENO schemes should be mostly centered. This implies that the algorithm may not be implemented in the *expanding-wavefront* manner as in the fast marching method [20, 22] and the group marching method [11]; it should be implemented with the *expanding-box* scheme. However, the expanding-box scheme is unstable for turning rays. To overcome the instability, Kim and Cook [15] has introduced a systematic framework for a dynamic *down-n-out* (DNO) marching and *post sweeping* (PS) iteration. DNO was originally suggested by Vidale [23] for the traveltimes computation with a predetermined order of down and out combination, which was adopted later by Dellinger and Symes [2]. Incorporating a dynamic (and automatic) combination of down and out marchings, DNO has improved its performance in both efficiency and accuracy [5, 15]. Instability that is still remained after the dynamic DNO marching could be cured by the PS iteration, in which ENO-RK2 (A.5) is applied in various directions, with the pseudo-temporal variable replaced correspondingly, to update the traveltimes by choosing the minimum among those computed solutions. Such an iteration strategy, *DNO-PS*, has been successfully tested for various velocity models having large contrasts as in those of the Gulf of Mexico. Details of DNO-PS and efficient implementation strategies can be found in Kim and Cook [15] and Kim [5, 7, 8].